

A scaling law for aeolian dunes on Mars, on Earth and subaqueous ripples

Philippe Claudin and Bruno Andreotti

*Laboratoire de Physique et Mécanique des Milieux Hétérogènes (UMR CNRS 7636),
ESPCI, 10 rue Vauquelin, 75231 Paris Cedex 05, France.*

Abstract

The linear stability analysis of equations governing the evolution of a flat sand bed submitted to a shearing flow predicts that the wavelength λ at which the bed destabilises to form dunes should scale with the drag length $L_{drag} = \frac{\rho_s}{\rho_f} d$. We tested this scaling law using measurements performed in water (subaqueous ripples), in air (aeolian dunes) and in the CO₂ martian atmosphere (martian dunes). The main difficulty is to determine the diameter of saltating grains on Mars. A first estimation comes from photographs of aeolian ripples taken by the rovers Opportunity and Spirit, showing grains whose diameters are smaller than on Earth dunes. In addition we calculate the effect of cohesion on the saltation threshold. It confirms that the small grains visualised by the rovers should be (or have been) grains experiencing saltation. Finally, we show that, within error bars, the scaling of λ with L_{drag} holds over almost five decades. We conclude with a discussion on the time scales and velocities at which these bed instabilities develop and propagate on Mars.

Key words: dune, saltation, Mars, instability

PACS: 45.70.Qj (Pattern formation), 47.20.Ma (Interfacial instability), 96.30.Gc (Mars)

Aeolian sand dunes form appealing and photogenic patterns whose shapes have been classified as a function of wind regime and sand supply [1,2]. These dunes have martian ‘cousins’ with very similar features [3]. Grains can also be transported by water flows, and bed instabilities are commonly reported in rivers or sea chanel [4]. The same dynamical mechanisms control the formation of aeolian (both on Earth and Mars) dunes and subaqueous ripples¹ from a flat sand bed. In a first section we describe the framework in which

¹ Subaqueous ‘ripples’ are defined as patterns whose typical size is much smaller than the water height, whereas that of subaqueous ‘dunes’ is comparable to depth.

this instability can be understood. A unique length scale is involved into this description, namely the sand flux saturation length L_{sat} which scales with the drag length $L_{drag} = \frac{\rho_s}{\rho_f}d$, where d is the grain diameter and ρ_s/ρ_f the grain to fluid density ratio. It governs the scaling of the wavelength λ at which dunes or subaqueous ripples nucleate.

However, attempting to test the scaling laws governing aeolian sand transport and dunes characteristic size, one faces a major problem: the grain size does not vary much from place to place at the surface of Earth and the grain to air density ratio is almost constant. This narrow range of grain size composing these dunes has a physical origin: large grains are too heavy to be transported by the wind and very small ones – dust – remain suspended in air. As shown by Hersen *et al.* [5,6], small-scale barchan dunes can be produced and controlled under water, with a characteristic size divided by 800 – the water to air density ratio – with respect to aeolian dunes. The martian exploration and particularly the discovery of aeolian patterns (ripples, mega-ripples and dunes) give the opportunity to add a third experimental point to check transport scaling laws, as the martian atmosphere is typically 60 to 80 times lighter than air.

The main difficulty is to determine the diameter of saltating grains on Mars. A first estimation comes from photographs of the soil taken by the rovers Opportunity and Spirit next to ripple patterns, showing grains whose diameters are smaller than on Earth dunes [7]. We also calculate the effect of cohesion on the saltation threshold. It confirms that the small grains visualised by the rovers should be (or have been) grains experiencing saltation. Finally, we show that, within error bars, λ scales with L_{drag} over five almost decades and discuss the corresponding time scales and velocities at which these bed instabilities develop and propagate.

1 Dune instability

The instability results from the interaction between the sand bed profile, which modifies the fluid velocity field, and the flow that modifies in turn the sand bed as it transport grains. Let us consider a flat and symmetric bump as shown in figure 1. The fluid is accelerated on the upwind (stoss) side and decelerated on the downwind side. This is schematized by the flow lines in this figure: they are closer to each other on the bump. This results in an increase of the shear stress τ applied by the flow on the stoss side of the bump. Conversely, τ decreases on the lee side. Assuming that the maximum amount of sand that can be transported by a given flow – the *saturated* sand flux – is an increasing function of τ , erosion takes place on the stoss slope as the flux increases, and sand is deposited on the lee of the bump. If the velocity field was symmetric around the bump, the transition between erosion and deposition would be

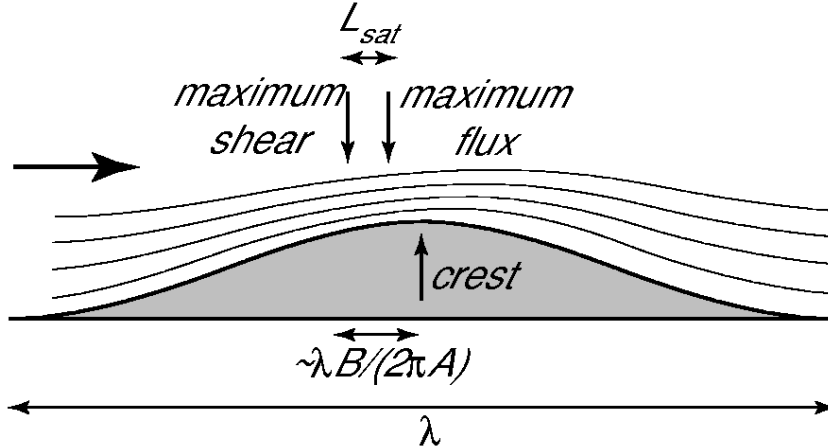


Fig. 1. Instability mechanism: a bump grows when the maximum flux is shifted upwind from the crest – the fluid flows from left to right; the stream lines around the bump are schematically drawn. The shift of the maximum shear stress scales with the size of the bump. The spatial lag between the shear and flux maxima is the saturation length L_{sat} .

exactly at the crest, and this would lead to a pure propagation of the bump, without any change in amplitude (we call this the ‘ A ’ effect, see below). In fact, due to the simultaneous effects of inertia and dissipation (viscous or turbulent), the velocity field is asymmetric (even on a symmetrical bump) and the position of the maximum shear stress is shifted upwind with respect to the crest of the bump (the ‘ B ’ effect). In addition, there is always a spatial lag for the sand transport to reach its saturated value; a separate dynamical effect. This relaxation process is characterised by a saturation length L_{sat} , and the maximum of the sand flux q is shifted downwind by a typical distance of order of L_{sat} from the point at which τ is maximum. The criterion of instability is then geometrically related to the position at which the flux is maximum with respect to the top of the bump: an up-shifted position leads to grains which start to be deposited before the crest, so that the bump grows.

The above qualitative arguments can be translated into a precise mathematical framework, see e.g. [8,9]. For a small deformation of the bed profile $h(t, x)$, the excess of stress induced by a non-flat profile can be written in Fourier space as:

$$\hat{\tau} = \tau_0(A + iB)k\hat{h}, \quad (1)$$

where τ_0 is the shear that would be felt on a flat bed and k is the wave vector associated to the spatial coordinate x . A and B are dimensionless functions of all parameters and of k in particular. The A part is in phase with the bed profile, whereas the B one is out of phase, so that the modes of h and τ with a wavelength λ have a spatial phase difference of the order of $\lambda B/(2\pi A)$. This shift is typically of the order of 10% of the length of the bump as A and B are typically of the same order of magnitude. Expressions for A and B have been derived by Jackson and Hunt [10] in the case of a turbulent flow. As shown

by Kroy *et al.* [11], A and B only weakly (logarithmically) depend on the wavelength so that they can be considered as constant for practical purpose (large dunes).

If the shear stress is below some threshold value τ_{th} , no transport is observed, hence the sand flux is null. Above this threshold, one observes on a flat bed a saturated flux Q which is a function of τ_0 . The fact that a wind of a given strength can only transport a finite quantity of sand is due to the negative feedback of the grains transported by the fluid on the flow velocity profile – the moving grains slow down the fluid. This saturation process of the sand flux is still a matter of research [12,13,14]. We refer the interested reader to [14,15] for review discussion. For our present purpose, we need a first order but quantitative description of the saturated flux. Following [14], Rasmussen *et al.* wind tunnel data [16] are well described by the relationship:

$$Q = 25 \frac{\tau_0 - \tau_{th}}{\rho_s} \sqrt{\frac{d}{g}} \quad \text{if } \tau_0 > \tau_{th} \quad \text{and} \quad Q = 0 \quad \text{otherwise.} \quad (2)$$

g is gravitational acceleration, and the prefactor 25 has been adjusted to fit the data, and is reasonably independent of the grain size d . The equivalent of the relation (1) for the saturated flux on a modulated surface q_{sat} can then be written as

$$\hat{q}_{sat} = Q(\tilde{A} + i\tilde{B})k\hat{h}, \quad (3)$$

where, by the use of relation (2), the values of \tilde{A} and \tilde{B} simply verify $A/\tilde{A} = B/\tilde{B} = 1 - \tau_{th}/\tau_0$.

As for any approach to an equilibrium state, there exists a relaxation length – or equivalently time – scale associated with the sand flux saturation. This was already mentioned by Bagnold who measured the spatial lag needed by the flux to reach its saturated value on a flat sand patch [17]. A saturation length L_{sat} in dune models has been first introduced by Sauermann *et al.* [18], where the dependence of L_{sat} with τ and in particular its divergence as $\tau \rightarrow \tau_{th}$ has been put phenomenologically in the description. In fact, this saturation length should *a priori* depend on the mode of transport. In the eolian turbulent case, the theoretical analysis in [14] shows that it should scale as $L_{sat} = L_{drag} \mathcal{F}(\tau_0/\tau_{th})$, where the drag length $L_{drag} = \frac{\rho_s}{\rho_f} d$ is the length needed for a grain in saltation to be accelerated to the fluid velocity, and \mathcal{F} a dimensionless function. Andreotti showed that the divergence of \mathcal{F} as $\tau_0 \rightarrow \tau_{th}$ is effective only very close to the threshold, and that in the range of physical interest, L_{sat} can also be considered as constant [14]. Using data collected in a dune field in the Maroccan atlantic Sahara [9], we compute the prefactor between L_{sat} and L_{drag} and get

$$L_{sat} \simeq 4.4 \frac{\rho_s}{\rho_f} d. \quad (4)$$

This result is also consistent with Bagnold’s data [17]. In the case of bed load driven by a turbulent water flow, there is no available information but it is reasonable to similarly identify the saturation length with the drag length up to some prefactor.

The linear stability analysis of the coupled differential equations of this framework has been performed in [8]. In particular, the wavenumber corresponding to the maximum growth rate is given by

$$k_{max} L_{sat} = \frac{\left(\frac{\tilde{A}}{\tilde{B}}\right)^{1/3}}{\left[-9 + 3\sqrt{3}\sqrt{1 + \left(\frac{\tilde{A}}{\tilde{B}}\right)^2}\right]^{1/3}} - \frac{\left[-9 + 3\sqrt{3}\sqrt{1 + \left(\frac{\tilde{A}}{\tilde{B}}\right)^2}\right]^{1/3}}{3\left(\frac{\tilde{A}}{\tilde{B}}\right)^{1/3}}. \quad (5)$$

For typical values of \tilde{A} and \tilde{B} we used in the barchan dune context [9], we have $\lambda_{max} = 2\pi/k_{max} \sim 12L_{sat}$. Note that we have $A/B = \tilde{A}/\tilde{B}$, so that $k_{max} L_{sat}$ is independent of τ_0 and τ_{th} . Using measurements in water (subaqueous ripples), in air (aeolian dunes) and in the CO₂ martian atmosphere (martian dunes), we investigate the scaling relation between λ_{max} and L_{drag} . To do so, we now need an estimation of the size of saltating grains on Mars.

2 Size of saltating grains on Mars

The determination of the typical size of the grains participating in saltation on martian dunes is a challenging issue. First, the dunes seem to evolve very slowly or may even have become completely static. Second, no sample of the matter composing the bulk of the dunes is available. Third, we do know from the observation of dunes on Earth that they can be covered by larger grains that do not participate to the transport in saltation. With the two rovers Opportunity and Spirit, we now have direct visualisations of the soil [7], in particular of clear aeolian structures like ripples² or nabkhas³. Unfortunately, these structures did not lay on the surface of a dune. We thus analyze the available photographs, assuming that, like on Earth, the size of the grains participating in saltation does not vary much from place to place.

² Contrarily to dunes, aeolian sand ripples form by a screening instability related to geometrical effects [17].

³ As there is a reduction of pressure in the lee of any obstacle, sand accumulates in the form of streaks aligned in the direction opposite to the wind (shadow dunes). These structures are called nabkhas [19].

2.1 Direct measurement of grain sizes

The photographs freely accessible online are not of sufficiently good resolution to determine the shape and the size of each grain composing the surface. Besides, one has to be careful when analyzing such pictures as part of what is visible at the surface corresponds to grains just below it and partly hidden by their neighbours. We have thus specifically developed a method to determine the average grain size in zones where the grains are reasonably monodispersed, when the resolution is typically larger than 3 pixels per grain diameter. This measure can be deduced from the computation of the auto-correlation function $C(\delta)$ of the picture, which decreases typically over one grain size. More precisely, we proceed with the following procedure:

- The zones covered by anything but sand (e.g. gravels or isolated larger grains) are localized and excluded from the analysis.
- Because in natural conditions the light is generally inhomogeneous, we perform a local smoothing of the picture with a gaussian kernel of radius $\simeq 10 d$. The resulting picture is subtracted from the initial one.
- We compute the local standard deviation of this image difference with the same gaussian kernel and produce, after normalisation, a third picture \mathcal{I} of null local average and of standard deviation unity.
- The auto-correlation function $C(\delta)$ is computed on this resulting picture, averaging over all directions:

$$C(\delta) = \frac{\sum_{k,l/k^2+l^2=\delta^2} \sum_{i,j} \mathcal{I}_{i,j} \mathcal{I}_{i+k,j+l}}{\sum_{k,l/k^2+l^2=\delta^2} \sum_{i,j} 1} \quad (6)$$

Figure 2a shows the curve $C(\delta)$ obtained from a series of photographs of aeolian sand sampled on a terrestrial dune. For all the resolutions used (between 1 and 5 pix/ d), the data collapse on a single curve, which is thus characteristic of the sand sample. The top inset shows the distribution of size, weighted in mass, in log-log representation. It presents a narrow peak around the d_{50} value. The autocorrelation function decreases from 1 to 0 over a size of the order of d_{50} (Lorenzian fit). We assume that this curve is in fact a function of δ/d_{50} only. This means that one can use it as a reference for the martian case. Figure 2b shows the autocorrelation curve obtained from the colour image taken by the rover Spirit at its landing site. $C(\delta)$ decreases faster than the reference curve but by tuning the value of the martian d_{50} , one can superimpose the Mars data with the solid line fairly well. From this picture as well as a series of gray level photographs taken by the rover Opportunity, we have estimated the diameter of the grains composing these aeolian formations to $87 \pm 25 \mu\text{m}$.

The first measurement of martian grain sizes dates back to the Viking mission in the 70s. On the basis of thermal diffusion coefficient measurements, Edgett and Christensen have estimated the grain diameter to be around $500 \mu\text{m}$ and

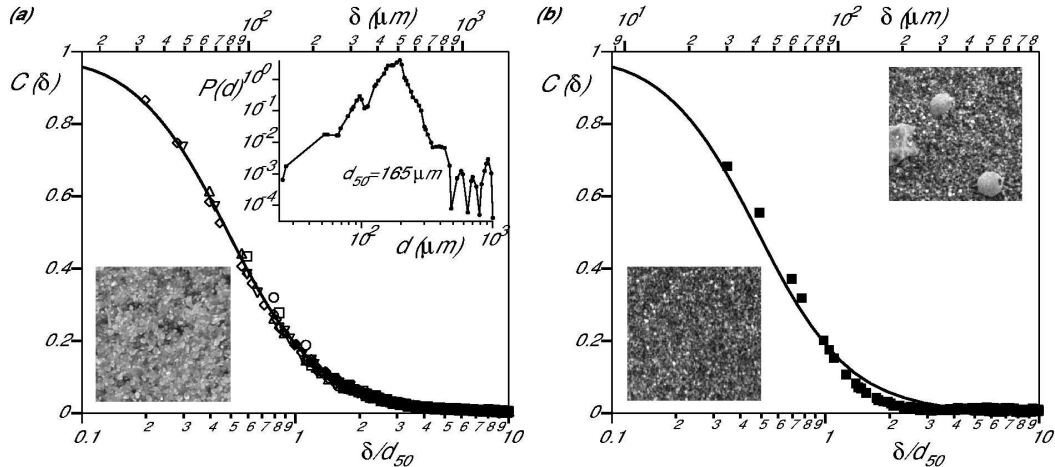


Fig. 2. Measurement of the typical grain size from the auto-correlation function $C(\delta)$ of a photograph of the granular bed. **a** Sample of aeolian sand from the mega-barchan of Sidi-Aghfinir (Atlantic Sahara, Morocco), of typical diameter $d \simeq 165 \mu\text{m}$. Top inset: Probability distribution function of the grain diameter d , weighted in mass. The narrow distribution around the maximum of probability is characteristic of the aeolian sieving process. Bottom inset: $200 \times 200 \text{ pix}^2$ zoom on a typical photograph on which the computation of the autocorrelation function has been performed. The image resolution is here $5 \text{ pix}/d$. **b** Sample of sand from Mars (at rover Spirit's landing site: 16.6° S , 184.5° W). Top inset: photograph showing the presence of millimetric grains as well as much smaller ones which are expected to be the saltans. Bottom inset: same as **a**, but the typical image resolution is $3 \text{ pix}/d$.

at least larger than those composing dunes on Earth [20]. This size corresponds to larger grains than saltans such as those shown in the top inset of figure 2b. In agreement with our findings, wind tunnel experiments performed in 'martian conditions' [21] have shown that grains around $100 \mu\text{m}$ are the easiest to dislodge from the bed (see also next subsection).

Several theoretical investigations of the size of aeolian martian grains have been conducted, starting with the work of Sagan and Bagnold [22]. In this paper the authors argue that, as Mars is a very arid planet, the cohesion forces due to humidity can be neglected and proposed a cohesion-free computation which predicts that very small grains (typically of one micron) may be put into saltation. Miller and Komar [23] also followed this cohesion-free approach and proposed transport threshold curves with no turnup on small particle size. It was soon realized that cohesion forces can occur for reasons other than humidity – namely van der Waals forces – and several authors proposed transport threshold curves with a peaked minimum around $100 \mu\text{m}$ [24,25,26,27,28]. However in these papers, cohesion is treated in an empirical fashion, with the assumption that van der Waals forces lead to an attractive force proportional to the grain diameter with a prefactor independent of d . We shall then reconsider below at a more fundamental level the scaling laws for

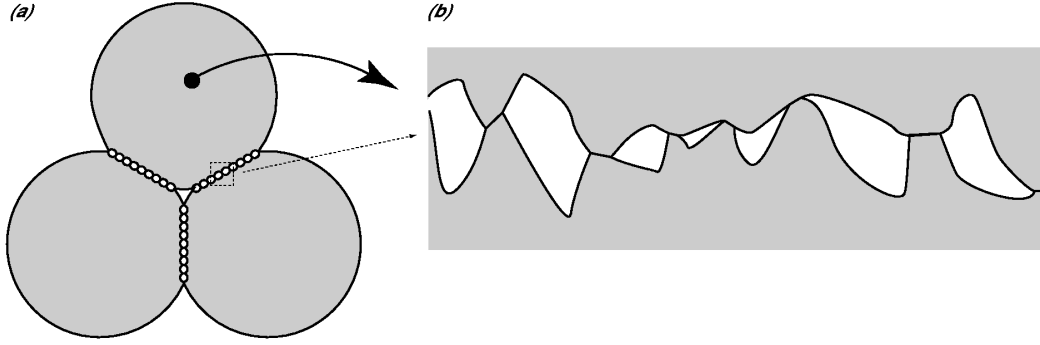


Fig. 3. **a** Grain packing geometry considered for the computation of transport thresholds. **b** Schematic drawing showing the contact between grains at the micron scale.

transport thresholds with, in particular, a detailed analysis of cohesion effects.

2.2 Transport thresholds

We consider the generic case of a fluid boundary layer over a flat bed composed of identical sand grains. For given grains and surrounding fluid, the shear stress τ controls the sand transport: below a threshold τ_{th} , there is no transport and above it grains are dragged from the bed and brought into motion. The dominant mechanism for grain erosion depends on the sand to fluid density ratio. In dense fluids grains are directly entrained by the flow whereas in low density fluids grains are mostly splashed up by other grains impacting the sand bed. Furthermore, when the fluid velocity increases, more and more grains remain in suspension in the flow, trapped in velocity fluctuations. As a consequence, the physics of the transport threshold is different for bed load (or ‘tractation’) and for saltation.

As tractions do not rebound, the threshold shear velocity associated with the bed load is that for which the grains trapped in the bed are directly entrained by the fluid. The threshold shear velocity associated with saltation/reptation is that for which one grain ejected by another grain (a repton) and accelerated by the undisturbed wind produces statistically one ejected grain after collision with the bed – the so-called replacement capacity is equal to 1. This dynamical threshold is lower than that associated to tractation in the case of large density contrast between the fluid and the grains [14]. This difference is responsible for the transport hysteresis observed in the eolian case. However, even if reptation and saltation further develop, the very initial motion of grains must be by direct fluid entrainment.

The bed load threshold is directly related to the fact that the grains are trapped in the potential holes created by the grains at the sand bed surface.

To get the scaling laws, the simplest geometry to consider is a single spherical grain jammed between the two neighbouring (fixed) grains below it, see figure 3a. Let us first discuss the situation in which the cohesive forces between the grains are negligible and the friction at the contacts is sufficient to prevent sliding. It can be inferred from figure 3a that the loss of equilibrium occurs for a value of the driving force F proportional to the submerged weight of the grain: $F \propto (\rho_s - \rho_f)gd^3$, where ρ_s is the mass density of the sand grain, and ρ_f is that of the fluid – which is negligible with respect to ρ_s in the case of aeolian transport. As F is proportional to the shear force τd^2 exerted by the fluid, the non-dimensional parameter controlling the onset of motion is the Shields number, which characterises the ratio of the driving shear stress to the normal stress:

$$\Theta = \frac{\tau}{(\rho_s - \rho_f)gd}. \quad (7)$$

The threshold value can be estimated from the geometry of the piling, and depends on whether rolling or lifting is the mechanism which makes the grain move. Experimentally, a typical value of the threshold Shields number is $\Theta_{th} \sim 0.01$ [2]. Finally, the local slope of the bed modifies the threshold value as traps between the grains are less deep when the bed is inclined. In particular, its value must vanish as the bed slope approaches the (tangent of the) avalanche angle. We here ignore these refinements which can be incorporated into the values of A and B .

For small grains, the cohesion of the material strongly increases the threshold shear stress. Evaluating the adhesion force between grains is a difficult problem in itself. We consider here two grains at the limit of separation and we assume that the multi-contact surface between the grains has been created with a maximum normal load N_{max} , see figure 3b. The adhesion force N_{adh} can be expressed as an effective surface tension $\tilde{\gamma}$ times the radius of curvature of the contact, which is assumed to scale on the grain diameter d :

$$N_{adh} \propto \tilde{\gamma}d. \quad (8)$$

This effective surface tension is much smaller than the actual one, γ , as the real area of contact A_{real} is much smaller than the apparent one A_{Hertz} :

$$\tilde{\gamma} = \gamma \frac{A_{real}}{A_{Hertz}}. \quad (9)$$

The apparent area of contact can be computed following Hertz law for two spheres in contact under a load N_{max} :

$$A_{Hertz} \propto \left(\frac{N_{max}d}{E} \right)^{2/3}, \quad (10)$$

where E is the Young modulus of the grain [29]. To express the real area of contact, we need to know whether the micro-contacts are in an elastic or

	Earth \earth	Mars \mars	Earth/Mars	water \water	air/water
g	9.8 m/s ²	3.7 m/s ²	2.7	9.8 m/s ²	1
λ	20 m	600 m	1/30	2 cm	1/800
d	165 – 180 μm	87 μm		150 μm	
ρ_f	1.2 kg/m ³	1.5 – 2.2 10^{-2} kg/m ³	60 – 80	10 ³ kg/m ³	1/830
ρ_s	2650 kg/m ³	3000 kg/m ³	0.9	2650 kg/m ³	1

Table 1

Comparison of different quantities (gravity g , initial wavelength of bed instability λ , diameter of saltons d and fluid and sediment densities ρ_f and ρ_s) in the air (Earth), in the martian atmosphere and in water. As the temperature at the surface of Mars can vary by an amplitude of typically 100 K between warm days and cold nights, the density of the atmosphere displays some variation range.

a plastic regime. Within a good approximation, A_{real} can expressed in both cases [30] as

$$A_{real} \propto \frac{N_{max}}{M}, \quad (11)$$

where M is the Young modulus E (elastic regime) or the hardness H (plastic regime) of the material. Altogether, we then get:

$$N_{adh} \propto \gamma \frac{E^{2/3}}{M} (N_{max}d)^{1/3}. \quad (12)$$

In order to bring into motion such grains, the shear must be large enough to overcome both weight and adhesion, so that, for $N_{max} \sim \rho_s g d^3$ (i.e. the weight of one grain) the critical Shields number is the sum of two terms and takes the form of

$$\Theta_{th} = \Theta_{th}^{\infty} \left[1 + \frac{3}{2} \left(\frac{d_m}{d} \right)^{5/3} \right], \quad (13)$$

where Θ_{th}^{∞} is the critical Shields number without any attractive force between the grains, and

$$d_m \propto \left(\frac{\gamma}{M} \right)^{3/5} \left(\frac{E}{\rho_s g} \right)^{2/5}. \quad (14)$$

Note that, by contrast to the previous literature cited above, we find that the adhesive force finally scales with $d^{4/3}$ and the critical Shields number with $d^{-5/3}$ (instead of exponents 1 and -2 respectively).

Translated into shear velocity $u_*^2 \equiv \tau_{th}/\rho_f \simeq (\rho_s/\rho_f) g d \Theta_{th}$, it is easy to show that d_m corresponds to the size of the grains which move at the lowest velocity. On Earth, d_m is estimated to $\sim 60 \mu\text{m}$ [19] for which the shear velocity u_* is of the order of 0.16 m/s. The exact nature of martian sand grains is presently

unknown. Some recent work suggests that they are primarily basaltic with a density $\rho_s \sim 3000 \text{ kg/m}^3$ [31] which is just slightly larger than the typical sand grain densities on Earth. We make the assumption that all unknown parameters (γ , E , H , ...) are similar to those on Earth, so that fluid density as well as gravity are the main important factors – see table 1. One can then write

$$d_{\sigma_m} = \left(\frac{g\delta \rho\delta_s}{g\sigma \rho\sigma_s} \right)^{2/5} \quad d_{\delta_m} \sim 85 \text{ } \mu\text{m}, \quad (15)$$

which corresponds to $u_* \sim 1 \text{ m/s}$. In figure 4 is plotted the shear velocity as a function of d . It diverges as $d \rightarrow 0$, and increases gently at large d . Below this line, no motion is possible. On the same graph, we also represented the settling velocity $u_{fall}(d)$ defined as the velocity for which $\Theta = 1$ [17]. This line is in fact a smooth crossover above which grains remain in suspension, so that saltation occurs between the two lines.

As a matter of fact, $u_* \sim 1 \text{ m/s}$ is already quite a large value. It corresponds to $u \sim 40 \text{ m/s}$ at 10 m. This value is consistent with the recent martian wind speed estimate by Jerolmack *et al.* [31]. It is then not surprising to find that the mobile grains on Mars such as those of figure 2b have a diameter close to d_m . This calculation thus suggests that the winds on Mars rarely exceed the strength needed to move grains.

3 A dune wavelength scaling law

Recalling that the wavelength λ which naturally appears when a flat sand bed gets destabilized by a shearing fluid scales with the flux saturation length, the idea is to plot λ against L_{drag} in the three different situations mentioned in the introduction, i.e. aqueous ripples as well as waves on aeolian dunes, both on Earth and Mars.

The study of small scale barchans under water [5,6] provides the first data point: measurement gives $\lambda \sim 2 \text{ cm}$ with glass beads of size $d = 150 \text{ } \mu\text{m}$, a size which leads to a drag length of $400 \text{ } \mu\text{m}$. An extensive work on the aeolian barchans of the Atlantic Sahara of Morocco and in particular on the way perturbations such as wind changes generate waves at their surface [9] gives $\lambda \sim 20 \text{ m}$. $L_{sat} \sim 1.7 \text{ m}$ was measured independently in the same dune field, and these aeolian grains of $180 \text{ } \mu\text{m}$ lead to a drag length of 40 cm . Figure 6a shows the histogram of the corresponding wavelength measurements. The solid line is peaked around its average value. When some coarsening can occur, as on the back of a mega-barchan (dashed line), the averaged λ can increase up to $\sim 28 \text{ m}$.

Recent photos of martian dunes [3] such as that in figure 5 lead to an estimate

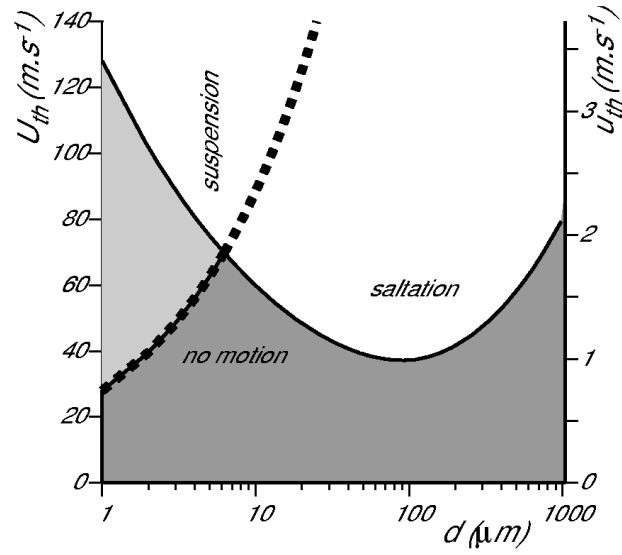


Fig. 4. Diagram showing the mode of transport on Mars as a function of the grain diameter d and of the wind speed expressed both at 10 m (left) from the soil and as a turbulent shear velocity (right).

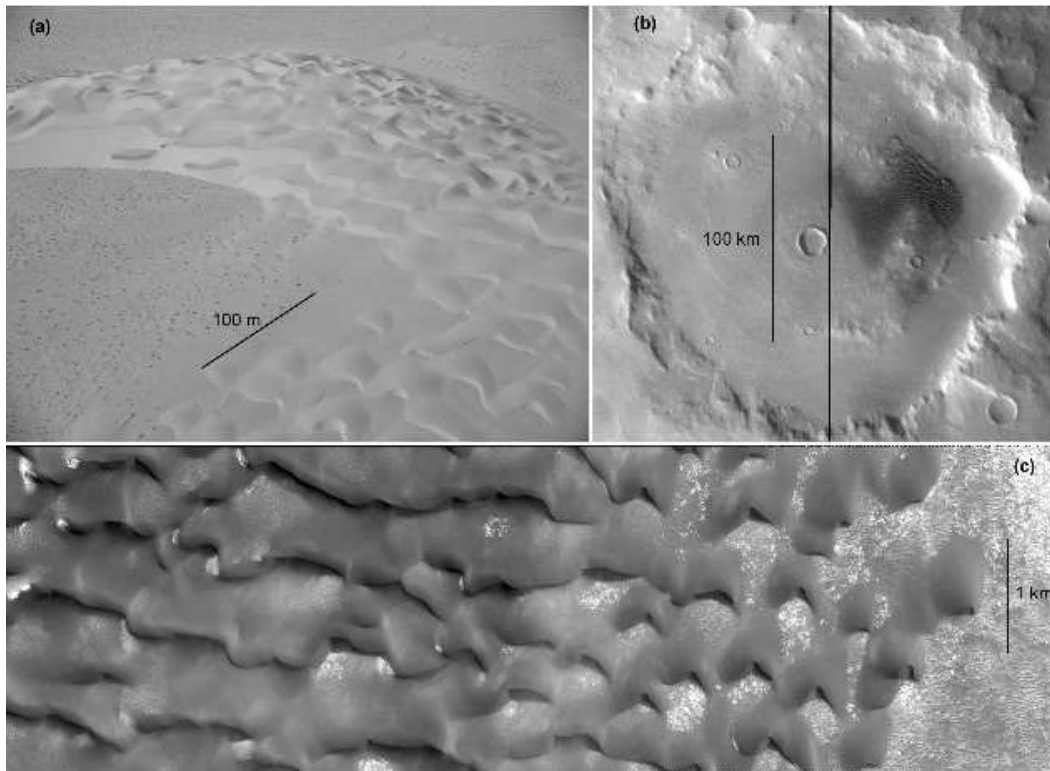


Fig. 5. Comparison of dune morphologies on Earth and on Mars. **a** Mega-barchan in Atlantic Sahara, Morocco. **b** 'Kaiser' crater on Mars ($341^{\circ}\text{W}, 47^{\circ}\text{S}$). **c** Closer view of the Kaiser crater dunes. As on Earth, small barchans are visible on the side of the field.

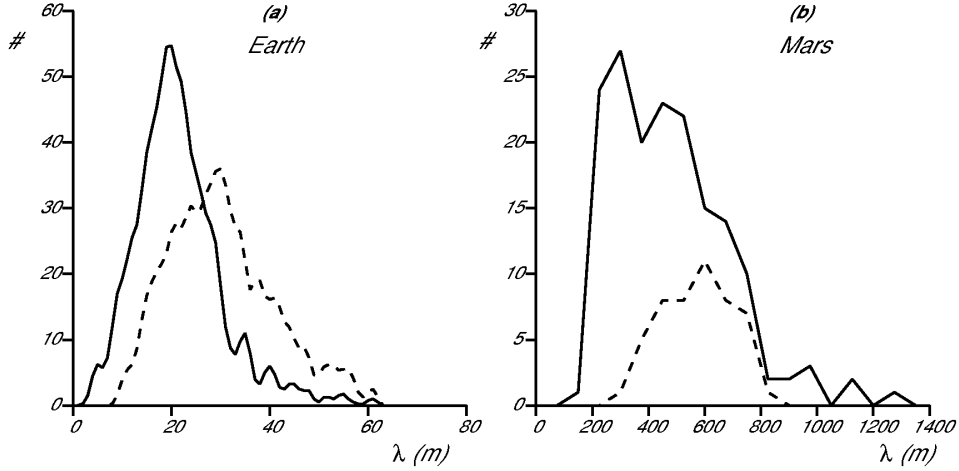


Fig. 6. Histograms of the wavelength measured in the Atlantic Sahara (Morocco) and in Mars southern hemisphere (mainly, but not only, in the region $320\text{--}350^\circ\text{W}$, $45\text{--}55^\circ\text{S}$). **a** Solid line: wavelengths systematically measured on barchan dunes located in a $20\text{ km} \times 8\text{ km}$ zone; Dash line: wavelengths measured on the windward side of a mega-barchan whose surface is permanently corrugated and where some coarsening occurred. **b** Solid line: wavelengths measured on dunes in several craters (e.g. Rabe, Russell, Kaiser, Proctor, Hellespontus); Dash line: histogram restricted to Kaiser crater (341°W , 47°S). Averaged values of λ are 20 m (**a** solid line), 28 m (**a** dash line), 510 m (**b** solid line) and 606 m (**b** dash line).

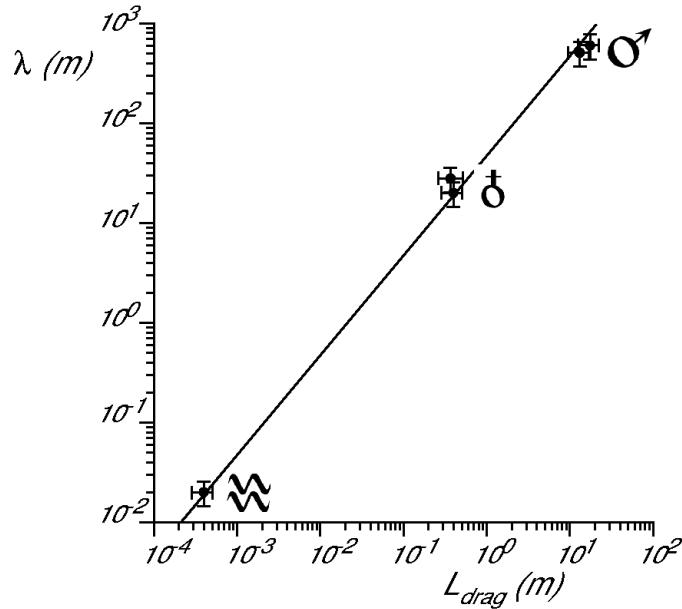


Fig. 7. Average wavelength as a function of the drag length. The two points labeled ‘Earth’ (resp. ‘Mars’) come from the two different histograms of figure 6a (resp. 6b). Error bars come from the width of these histograms. The data scattering due to the temperature variations of ρ_f on Mars is also shown as the L_{drag} of the two martian points have been computed for the two extremes values of the density range – see table 1.

of the value of $\lambda \sim 600$ m on Mars. We focused on the dunes found in craters of the southern hemisphere. For comparison, we have measured wavelengths on dunes in several craters (e.g. Rabe, Russell, Kaiser, Proctor, Hellespontus) and also produced a histogram restricted to Kaiser crater, see figure 6b. As for the drag length, we used the value for the grain diameter estimated in the previous section. As also mentioned above, the density of the martian grains can be estimated to be similar to that of terrestrial grains. The value of the density of the martian atmosphere however varies within some range as the temperature on Mars surface can change by an amplitude of typically 100 K between warm days and cold nights. In the end, it gives L_{drag} between 13 and 17 m. These data points are plotted in figure 7, showing a scaling law over almost five decades.

One may wish to add another data point in this scaling law. This could be possible using heavy and large grains under water, e.g. brass beads of $500 \mu\text{m}$ for which we expect a wavelength of the order of 10 cm. However, in order to remain in the regime where the free surface has no effect, a water tank of ~ 1 m depth is needed, which is beyond standard lab facilities.

4 Discussion: time scales and velocity for the martian dunes

Now that we have this unique length scale at hand for dunes, it is interesting to address the question of the corresponding growth time scales and propagation velocities. The linear stability analysis [8,9] tells that the growth rate σ and the propagation velocity c of bedforms are related to the wavenumber k as

$$\sigma(k) = Qk^2 \frac{\tilde{B} - \tilde{A}kL_{sat}}{1 + (kL_{sat})^2}, \quad (16)$$

$$c(k) = Qk \frac{\tilde{A} + \tilde{B}kL_{sat}}{1 + (kL_{sat})^2}, \quad (17)$$

where Q is the saturated sand flux – assumed constant – over a flat bed. In order to make these relations quantitative for the bedforms on Earth and Mars, we need an effective time averaged flux \bar{Q} . Recall from equation (2) that Q can be related to the shear stress τ_0 . For simplicity, we suppose that there is sand transport ($\tau_0 > \tau_{th}$) a fraction η of the time and that the shear stress is then constant and equal to $(1 + \alpha)\tau_{th}$. The time averaged sand flux can thus be effectively expressed as

$$\bar{Q} = 25 \sqrt{\frac{d}{g}} \frac{\tau_{th}}{\rho_s} \alpha \eta \propto \left[1 + \frac{3}{2} \left(\frac{d_m}{d} \right)^{5/3} \right] \left(1 - \frac{\rho_f}{\rho_s} \right) g^{1/2} d^{3/2} \alpha \eta. \quad (18)$$

The values of the coefficients \tilde{A} and \tilde{B} which come into equations (16) and (17) depend on the excess of shear above the threshold as $\tilde{A}/A = \tilde{B}/B = (1+\alpha)/\alpha$. The timescale over which an instability develops is that of the most unstable mode. This means that σ and c should be evaluated at $k = k_{max}$ (see equation (5)) and thus scale as:

$$\sigma \propto \frac{\bar{Q}}{L_{sat}^2} \propto \left[1 + \frac{3}{2} \left(\frac{d_m}{d} \right)^{5/3} \right] \left(\frac{\rho_f}{\rho_s} \right)^2 \left(1 - \frac{\rho_f}{\rho_s} \right) g^{1/2} d^{-1/2} (1 + \alpha) \eta, \quad (19)$$

$$c \propto \frac{\bar{Q}}{L_{sat}} \propto \left[1 + \frac{3}{2} \left(\frac{d_m}{d} \right)^{5/3} \right] \frac{\rho_f}{\rho_s} \left(1 - \frac{\rho_f}{\rho_s} \right) g^{1/2} d^{1/2} (1 + \alpha) \eta. \quad (20)$$

Using meteorological data and measurements of the average dune velocities, we estimate that Q_δ is between 60 to 90 m²/year [9] and η_δ between 65% and 85%. This gives an effective value α_δ between 1.5 and 2. Calculating explicitly the prefactors, we get a growth time $\sigma_\delta^{-1} \sim 2$ weeks and $c_\delta \sim 200$ m/year, which is consistent with direct observation. Note that time scales for individual fully developed dunes depend on their size, but are also proportional to $1/\bar{Q}$ [32].

We can now reach a conclusion about the characteristic time scale on Mars. It may be seen from equations (19) and (20) that the two most important factors are the atmosphere density ρ_f and the wind intermittency factor η . Indeed, the gravity and the grain size are of same order of magnitude on Earth and on Mars. This is consistent with White [33] who concluded that the saturated flux in the similar dynamic conditions is larger on Mars by a factor smaller than 10. As emphasized by the calculation of the transport threshold in the cohesive case, one expects that α_σ is of order unity at most. As a conclusion, ρ_s , g , d and α give subdominant contributions to the Mars to Earth ratios for σ and c so that:

$$\frac{\sigma_\sigma}{\sigma_\delta} \simeq \left(\frac{\rho_{\delta f}}{\rho_{\sigma f}} \right)^2 \frac{\eta_\sigma}{\eta_\delta}, \quad (21)$$

$$\frac{c_\sigma}{c_\delta} \simeq \frac{\rho_{\delta f}}{\rho_{\sigma f}} \frac{\eta_\sigma}{\eta_\delta}. \quad (22)$$

As the atmosphere density ratio $\rho_{\sigma f}/\rho_{\delta f}$ is of the order of 70, when squared, it induces a factor ~ 5000 on the time scale. The most speculative part naturally concerns the value of η_σ . As we saw that strong winds are needed to reach the threshold of transport, and as the soil of Mars is frozen during the winter season, one cannot expect sand transport more than few % of the time, and a realistic value is perhaps $\eta_\sigma \sim 0.01$, i.e. few days per year. This means that there are 4 to 5 decades between σ_σ and σ_δ . In other words, the typical time over which we could see an evolution of the bedforms on martian

dunes is of the order of several centuries to several thousand years. Similarly, the expected velocities should be several hundred times less than on Earth. Therefore, as some satellite high resolution pictures definitively show some evidence of aeolian activity – e.g. avalanche outlines – it may well be that the martian dunes are fully active but not significantly at the human scale.

We thank Éric Clément and Évelyne Kolb for useful advice on the way cohesion forces can be estimated. We thank Douglas Jerolmack for discussions. We thank Brad Murray for a careful reading of the manuscript. Part of this work is based on lectures given during the granular session of the Institut Henri Poincaré in 2005. This study was supported by an ‘ACI Jeunes Chercheurs’ of the french ministry of research.

References

- [1] S.G. Fryberger and G. Dean, in *A Study of Global Sand Seas* (McKee editor), Geol. Surv. Prof. Pap. 1052, Washington, 137 (1979).
- [2] K. Pye and H. Tsoar, *Aeolian sand and sand dunes*, Unwin Hyman, London (1990).
- [3] See photos on the web site http://barsoom.msss.com/moc_gallery/.
- [4] M.S. Yalin, *River mechanics*, Pergamon press, Oxford (1992).
- [5] P. Hersen, S. Douady and B. Andreotti, Phys. Rev. Lett. **89**, 264301 (2002).
- [6] P. Hersen, J. Geophys. Res. **110**, F04S07 (2005).
- [7] R. Sullivan *et al.*, Nature **436**, 58 (2005).
- [8] B. Andreotti, P. Claudin and S. Douady, Eur. Phys. J. B **28**, 341 (2002).
- [9] H. Elbelrhiti, P. Claudin and B. Andreotti, Nature **437**, 720 (2005).
- [10] P.S. Jackson and J.C.R. Hunt, Quart. J. R. Met. Soc. **101**, 929 (1975).
- [11] K. Kroy, G. Sauer mann and H.J. Herrmann, Phys. Rev. E **66**, 031302 (2002).
- [12] J.E. Ungar and P.K. Haff Sedimentology **34**, 289 (1987).
- [13] R.S. Anderson and P.K. Haff, Science **241**, 820 (1980).
- [14] B. Andreotti, J. Fluid Mech. **510**, 47 (2004).
- [15] R.S. Anderson and P.K. Haff, Acta Mechanica (suppl.) **1**, 21 (1991).
- [16] K.R. Rasmussen, J.D. Iversen and P. Rautahimo, Geomorphology **17**, 19 (1996).

- [17] R.A. Bagnold, *The physics of blown sand and desert dunes*, Methuen, London (1941).
- [18] G. Sauermann, K. Kroy and H.J. Herrmann, *Phys. Rev. E* **64**, 031305 (2001).
- [19] R. Cooke, A. Warren and A. Goudie, *Desert geomorphology*, UCL Press, London (1993).
- [20] K.S. Edgett and P.R. Christensen, *J. Geophys. Res.* **96**, 22765 (1991).
- [21] R. Greeley, R. Leach, B.R. White, J.D. Iversen and J.B. Pollack, *Geophys. Res. Lett.* **7**, 121 (1980).
- [22] C. Sagan and R.A. Bagnold, *Icarus* **26**, 209 (1975).
- [23] M.C. Miller and P.D. Komar, *Sedimentology* **24**, 709 (1977).
- [24] J.D. Iversen, J.B. Pollack, R. Greeley and B.R. White, *Icarus* **29**, 381 (1976).
- [25] J.B. Pollack, R. Haberle, R. Greeley and J.D. Iversen, *Icarus* **29**, 395 (1976).
- [26] J.D. Iversen and B.R. White, *Sedimentology* **29**, 111 (1982).
- [27] Y. Shao and H. Lu, *J. Geophys. Res.* **105**, 22437 (2000).
- [28] W.M. Cornelis, D. Gabriels and R. Hartman, *Geomorphology* **59**, 43 (2004).
- [29] K.L. Johnson, *Contact mechanics*, Cambridge University Press, Cambridge (1985).
- [30] J.-M. Georges, *Frottement, usure et lubrification*, Eyrolles, Paris (2000).
- [31] D.J. Jerolmack, D. Mohrig, J.P. Grotzinger, D.A. Fike and W.A. Watters, to appear in *J. Geophys. Res.*
- [32] P. Hersen, H. Elbelrhiti, K.H. Andersen, B. Andreotti, P. Claudin and S. Douady, *Phys. Rev. E* **69**, 011304 (2004).
- [33] B.R. White, *J. Geophys. Res.* **84**, 4643 (1979).